Stellar Clusters & Associations: A RIA Workshop on Gaia
Granada, 23rd - 27th May 2011

Radiative Feedback in Massive Star and Cluster Formation

Thomas Peters[1], Ralf S. Klessen[1], Mordecai-Mark Mac Low[2], and Robi Banerjee[1,3]

[1] Zentrum für Astronomie der Universität Heidelberg, Institut für Theoretische Astrophysik, Albert-Ueberle-Str. 2, D-69120 Heidelberg, Germany
[2] Department of Astrophysics, American Museum of Natural History, 79th Street at Central Park West, New York, New York 10024-5192, USA
[3] Hamburger Sternwarte, Gojenbergsweg 112, D-21029 Hamburg, Germany

Abstract

Understanding the origin of high-mass stars is central to modern astrophysics. We shed light on this problem with simulations using a novel, adaptive-mesh, ray-tracing algorithm. These simulations consistently follow the gravitational collapse of a massive molecular cloud core, the subsequent build-up and fragmentation of the accretion disk surrounding the nascent star, and, for the first time, the interaction between its intense UV radiation field and the infalling material. We show that ionization feedback can neither stop protostellar mass growth nor suppress fragmentation. We discuss the effects of feedback by ionizing and non-ionizing radiation on the evolution of the stellar cluster. The accretion is not limited by radiative feedback but by the formation of low-mass companions in a process we call "fragmentation-induced starvation". This behavior consistently reproduces the observed relation between the most massive star and the total mass of stars in a cluster. We show that magnetic fields reduce the star formation rate and lead to the formation of more massive stars.

1 Introduction

High-mass stars form in denser and more massive cloud cores (Motte et al., 2008) than their low-mass counterparts (Myers et al., 1986). High densities also result in local gravitational instabilities in the accretion flow, resulting in the formation of multiple additional stars (Klessen & Burkert, 2000; Kratter & Matzner, 2006). Young massive stars are almost always observed to have companions (Ho & Haschick, 1981), and the number of their companions significantly exceeds those of low-mass stars (Zinnecker & Yorke, 2007). Such companions

influence subsequent accretion onto the initial star (Krumholz et al., 2009). Observations show an upper mass limit of about $100\,\mathrm{M}_\odot$. It remains unclear whether limits on internal stability or termination of accretion by stellar feedback determines the value of the upper mass limit (Zinnecker & Yorke, 2007).

The most significant differences between massive star formation and low-mass star formation seem to be the clustered nature of star formation in dense accretion flows and the ionization of these flows. We present the first three-dimensional simulations of the collapse of a molecular cloud to form a cluster of massive stars that include ionization feedback by Peters et al. (2010a,c,b, 2011), allowing us to study these effects simultaneously.

2 Numerical Method and Initial Conditions

We present the first three-dimensional, radiation-(magneto-)hydrodynamical simulations of massive star formation, taking into account heating by both ionizing and non-ionizing radiation, using the adaptive-mesh code FLASH (Fryxell et al., 2000). We propagate the radiation on the adaptive mesh with our extended version of the hybrid characteristics raytracing method (Rijkhorst et al., 2006; Peters et al., 2010a). We use sink particles (Federrath et al., 2010) to model young stars. Sink particles are inserted when the Jeans length of collapsing gas can no longer be resolved on the adaptive mesh. They continue to accrete any high-density gas lying within their accretion radius. We use the sink particle mass and accretion rate to determine the radiation feedback with a prestellar model (Peters et al., 2010a). A detailed description of our numerical method and the underlying assumptions can be found in Peters et al. (2010a).

We start our simulations with a $1000\,M_\odot$ molecular cloud having a constant density core with $\rho = 1.27 \times 10^{-20}\ \mathrm{g\,cm^{-3}}$ within a radius of $r = 0.5\,\mathrm{pc}$, surrounded by an $r^{-3/2}$ density fall-off out to $r = 1.6\,\mathrm{pc}$. The cloud rotates as a solid body with an angular velocity $\omega = 1.5 \times 10^{-14}\,\mathrm{s^{-1}}$. The initial temperature is $T = 30\,\mathrm{K}$. The highest resolution cells on our adaptive mesh have a size of 98 AU. Sink particles are inserted at a cut-off density of $\rho_\mathrm{crit} = 7 \times 10^{-16}\,\mathrm{g\,cm^{-3}}$ and have an accretion radius of $r_\mathrm{sink} = 590\,\mathrm{AU}$.

We compare the results of four different simulations. In the first simulation (Run A), a dynamical temperature floor is introduced to suppress secondary fragmentation. Only one sink particle (representing a massive protostar) is allowed to form. In the second simulation (Run B), secondary fragmentation is allowed, and many sink particles form, representing a group of stars, each contributing to the radiative feedback. The third simulation (Run D) is a control run in which secondary fragmentation is still allowed, but no radiation feedback is included. The fourth simulation (Run E) is a magnetized version of Run B, the full stellar group simulation with radiation feedback from all stars. Run E includes an initially homogeneous magnetic field along the rotation axis of the cloud with a magnitude of $10\,\mu\mathrm{G}$, corresponding to a mass-to-flux ratio $(M/\Phi) = 14(M/\Phi)_\mathrm{cr}$ in the central core at the beginning of the simulation. See Peters et al. (2010b) and Peters et al. (2011) for a thorough discussion of these initial conditions.

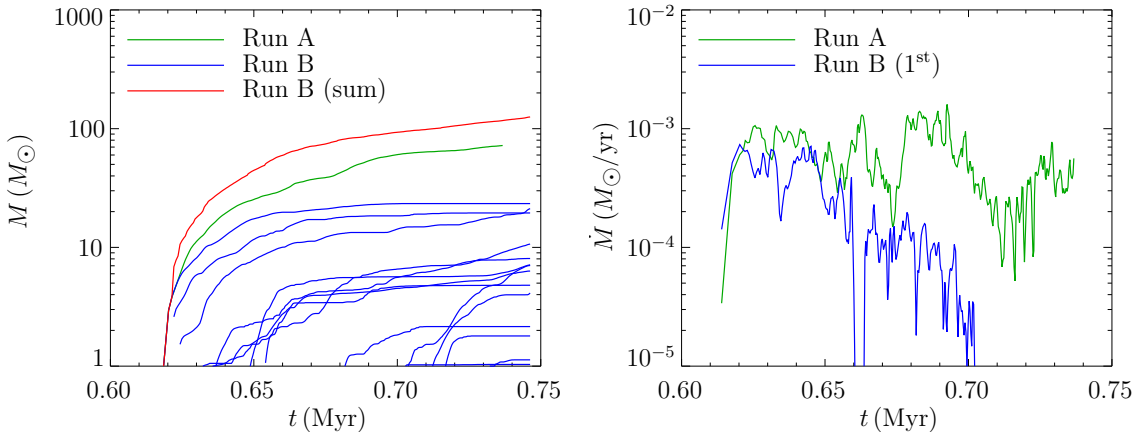

Figure 1: Accretion history of the single (Run A) and multiple (Run B) sink simulations. Run A was stopped at $72\,\mathrm{M}_\odot$, while no sink particle in Run B exceeds $25\,\mathrm{M}_\odot$ over the simulation runtime. The left hand plot shows the sink particle masses for Run A (green), the individual sink masses of Run B (blue) as well as the total mass in sink particles in Run B (red). The right hand plot shows the accretion rates of the sink particle in Run A (green) and the sink particle which forms first in Run B (blue), which also turns out to end up as the most massive at the end of the simulation. While the accretion rate in Run A never drops below $10^{-5}\,\mathrm{M}_\odot\,\mathrm{yr}^{-1}$, accretion onto the most massive sink can drop significantly below this value and even be stopped totally in Run B.

3 Fragmentation-Induced Starvation

We first examine the accretion histories of our different models. Figure 1 shows that in Run A, with only one sink particle allowed to form, nothing halts accretion onto the central protostar. It continues to grow at an average rate of $\dot{M} \approx 5.9 \times 10^{-4}\,\mathrm{M}_\odot\,\mathrm{yr}^{-1}$ until we stop the calculation when the star has reached $72\,\mathrm{M}_\odot$. The increasingly massive star ionizes the surrounding gas, raising it to high pressure. This gas breaks out above and below the disk plane, but it cannot halt mass growth through the disk[1] mid-plane.

In contrast, in Run B, where multiple sink particles are allowed to form, two subsequent sink particles form and begin accreting soon after the first one, and many more follow within the next $10^5\,\mathrm{yr}$ (see Figure 1). By that time the first sink has accreted $8\,\mathrm{M}_\odot$. Within another $3 \times 10^5\,\mathrm{yr}$ seven further fragments have formed, with masses ranging from $0.3\,\mathrm{M}_\odot$ to $4.4\,\mathrm{M}_\odot$ while the first three sink particles have masses between $10\,\mathrm{M}_\odot$ and $20\,\mathrm{M}_\odot$, all within a radius of $0.1\,\mathrm{pc}$ from the most massive object. Accretion by the secondary sinks terminates the mass growth of the central massive sinks. Material that moves inwards through the disk driven by gravitational torques accretes preferentially onto the sinks at larger radii (Bate, 2002). Eventually, hardly any gas makes it all the way to the center to fall onto the most massive objects. This fragmentation-induced starvation prevents any star from reaching a mass $> 25\,\mathrm{M}_\odot$ in this case.

[1]We will hereafter refer to the flattened, dense, accretion flow that forms in the midplane of our rotating core as a disk. However, it is not necessarily a true Keplerian, viscous, accretion disk, which probably only forms within the central few hundred astronomical units, unresolved by our models.

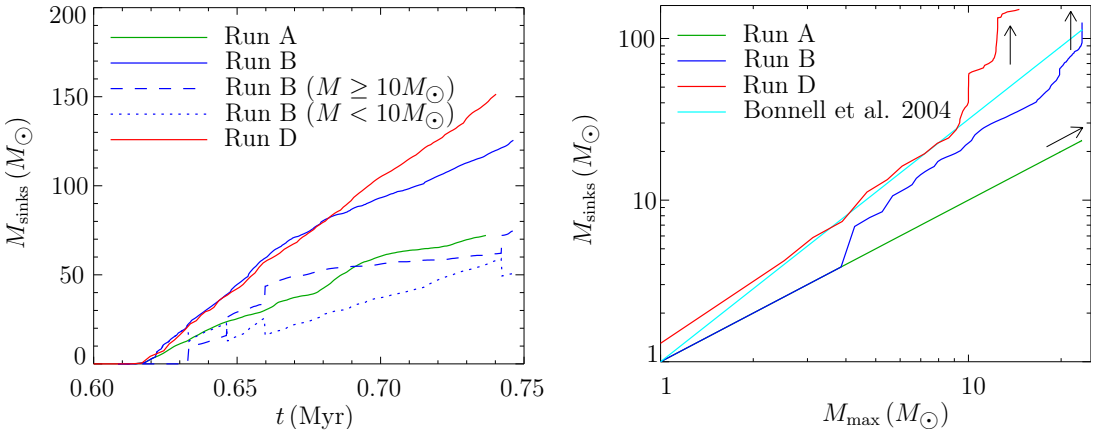

Figure 2: (*Left*) Total accretion history of all sink particles combined forming in Runs A, B, and D. While the heating by non-ionizing radiation does not affect the total star formation rate, the ionizing radiation appreciably reduces the total rate at which gas converts into stars once the most massive object has stopped accreting and its H II region can freely expand. The slope of the total accretion history in Run B goes down because the massive stars (dashed line) accrete at a decreased rate, while the low-mass stars (dotted line) keep accreting at the same rate. (*Right*) The total mass in sink particles $M_{\rm sinks}$ as a function of the most massive star in the cluster $M_{\rm max}$. We plot the curves for Run A, Run B and Run D as well as the fit from the competitive accretion simulations by Bonnell et al. (2004). The turn-off away from the scaling relation (indicated by arrows) is shifted towards higher masses by radiative feedback.

Figure 1 also reveals that the most massive stars in the cluster are those which form first and then keep accreting at a high rate. The most massive stars in Run B are the same for all times, but their mass keeps increasing during the formation of the stellar cluster.

The accretion behavior in Run B contrasts sharply with competitive accretion models (Bonnell et al., 2001, 2004), which have no mechanism to turn off accretion onto the most massive stars. In these models, material falls all the way down to the massive stars sitting in the center of the gravitational potential which thereby take away the gas from the surrounding low-mass stars. In our fragmentation-induced starvation scenario, exactly the opposite happens. Figure 2 illustrates that, although the accretion rates of the most massive stars ($M \geq 10\,{\rm M}_\odot$) steadily decrease, the low-mass stars ($M < 10\,{\rm M}_\odot$), keep accreting at the same rate.

Competitive accretion models show a correlation between the mass of the most massive star $M_{\rm max}$ and the total cluster mass $M_{\rm sinks}$ during the whole cluster evolution that is roughly $M_{\rm max} \propto M_{\rm sinks}^{2/3}$ (Bonnell et al., 2004). This correlation has been argued to represent a way to observationally confirm competitive accretion (Krumholz & Bonnell, 2009) and is in fact in good agreement with observations (Weidner & Kroupa, 2006; Weidner et al., 2010). However, we find that our simulations also reproduce the observed relation between $M_{\rm max}$ and $M_{\rm sinks}$.

Figure 2 shows $M_{\rm sinks}$ as function of $M_{\rm max}$ for Run A, Run B and Run D, and the relation $M_{\rm max} = 0.39 M_{\rm sinks}^{2/3}$, which was found by Bonnell et al. (2004) as a fit to their simulation data. Over the whole cluster evolution, the curve for Run D lies above this fit,

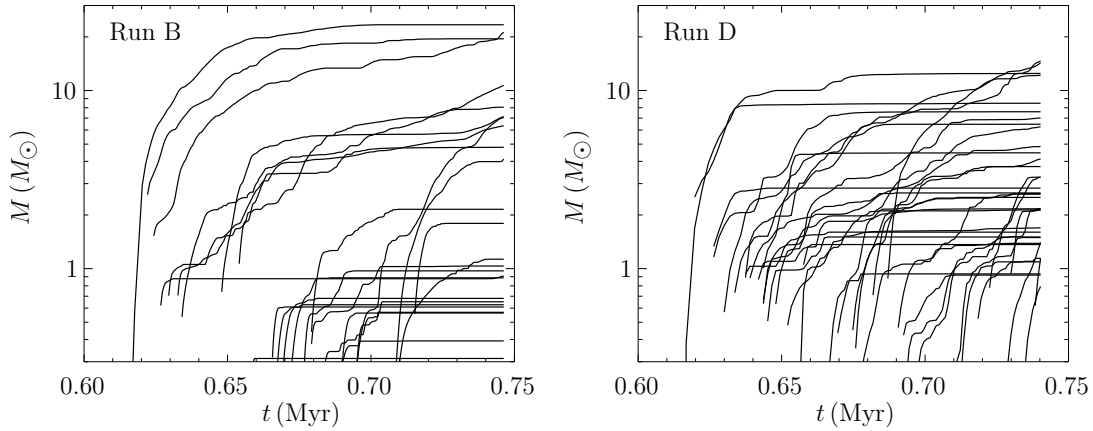

Figure 3: Individual accretion histories for Run B and Run D. The figure shows the stellar masses as function of time for all sink particles that form in Run B (*left*) and Run D (*right*). Because the Jeans mass is lower without radiative feedback (Run D), many more sink particles form in Run D than in Run B, and the mass of the most massive stars is also lower.

while the curve for Run B always lies below it. The fit agrees with our simulation data as well as it does to that of Bonnell et al. (2004). This indicates that the scaling is not unique to competitive accretion, but can also be found with the fragmentation-induced starvation scenario and hence cannot be used as an observational confirmation of competitive accretion models.

4 Effects of Radiative Feedback and Magnetic Fields

Figure 3 shows the individual accretion histories of each of the sink particles in Run B and Run D. Radiative heating cannot prevent disk fragmentation but raises the local Jeans mass. Hence, many fewer stars form in Run B than in Run D, and the mass of the most massive stars in Run B is higher. It is also evident from the figure that star formation is much more intermittent in the case with radiation feedback (Run B). The reason for this behavior is that the star formation process is controlled by the local Jeans mass, which depends to a large degree on how the filaments in the disk shield the radiation. Shielding can lower the Jeans mass temporarily and thereby allow gravitational collapse that would not have occurred otherwise.

Since the accretion heating raises the Jeans mass and length in Run B, the total number of sink particles is higher in Run D than in Run B, and the stars in Run D generally reach a lower mass than in Run B. These two effects cancel out to lead to the same overall star formation rate for some time (see Figure 2). At one point in the evolution, however, also the total accretion rate of Run B drops below that of Run D. At time $t \approx 0.68\,\mathrm{Myr}$ the accretion flow around the most massive star has attenuated below the value required to trap the H II region. It is able to break out and affect a significant fraction of the disk area. A comparison with the mass growth of Run D clearly shows that there is still enough gas available to continue constant cluster growth for another 50 kyr or longer, but the gas can no longer collapse in Run B. Instead, it is swept up in a shell surrounding the expanding H II

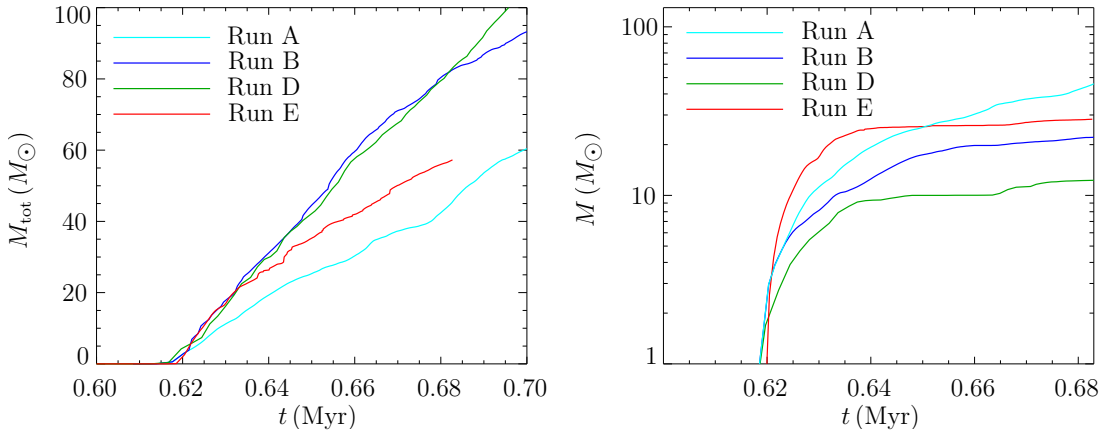

Figure 4: (*Left*) Total accretion history of Run A, Run B, Run D and Run E. While the total accretion rates of Run B and Run D agree until ionization feedback stops massive star formation in Run B, the total accretion rate in Run E already starts to decline after 20 kyr. The magnetic field in Run E additionally supports the gas against collapse, reducing the total accretion rate. (*Right*) Protostellar masses of the first sink particles in Run A, Run B, Run D and Run E. Radiative heating (Run B) and presence of magnetic fields (Run E) increase the final masses of the massive stars. The largest part of the additional mass accretion in Run E compared to Run B is due to the stronger initial accretion phase.

region.

It is also notable that the expanding ionization front around the most massive stars does not trigger any secondary star formation, which suggests that triggered star formation (Elmegreen & Lada, 1977) may not be as efficient as expected, at least on the scales considered here.

The total accretion histories of all sink particles combined in each of the four simulations are contrasted in Figure 4. For the first 20 kyr, the total accretion rate of Run B, Run D and Run E is nearly identical. The accretion rate in these multiple sink simulations is generally higher than in the single sink Run A since the large group of sinks accretes from a large volume, without needing to rely on outward angular momentum transport to deliver material to the direct feeding zone of the central sink. In the magnetized Run E, no secondary sink particles form during the first 20 kyr, so that the increased accretion rate in this phase is due to the additional angular momentum transport performed by the magnetic field. After the initial 20 kyr, the total accretion rate in Run E falls below Run B and the control Run D, deviating increasingly with time, but always staying above the accretion rate in Run A. The accretion histories of Run B and Run D only start to separate at relatively late time when the ionizing radiation begins to terminate accretion onto the most massive sinks in Run B (see the discussion in Peters et al. 2010b), but the magnetic field additionally reduces the rate at which gas collapses in Run E. Thus, the total accretion rate with magnetic fields is lower than without magnetic fields.

The central star in Run E can grow to larger masses because in the initial phase fragmentation is delayed by magnetic support. This allows the central object to maintain a high accretion rate for a longer time. Nevertheless, the accretion rate of the massive star in

Run E drops significantly when secondary sink particles form, since they form in a dense ring around the central massive sink and to some extent starve it of material, even though they never cut off accretion entirely.

The stronger initial accretion phase in Run E compared to Run B yields the main contribution to the larger final mass of the massive sink. The magnetic field very efficiently redistributes angular momentum, resulting in an increased radial mass flux through the high-density equatorial plane. Consequently, the initial accretion rate in the magnetized simulation (Run E) even lies considerably above the non-magnetized single sink calculation (Run A).

5 Conclusions

We have reviewed some of the results of our recent radiation-(magneto-)hydrodynamical simulations of massive star formation (Peters et al., 2010a,c,b, 2011), which for the first time simultaneously include the effect of heating by both ionizing and non-ionizing radiation. We find that ionization feedback is unable to stop protostellar mass growth. Instead, the mass of the most massive stars is limited by the formation of lower-mass companions in their gravitationally unstable accretion flow in a process we call fragmentation-induced starvation. Our numerical model reproduces the observed relation between the most massive star in a cluster and the total cluster mass. We find that heating by non-ionizing radiation decreases the total number of stars formed and increases the mass of the most massive stars, but does not change the total star formation rate. The star formation rate is reduced by ionizing radiation once the H II regions can steadily expand. Even initially very weak magnetic fields can markedly reduce the star formation rate by providing additional support against gravitational collapse and lead to the formation of more massive stars via magnetic braking of the accretion flow.

References

Bate, M. R. 2002, MNRAS, 314, 33

Bonnell, I. A., Bate, M. R., Clarke, C. J., & Pringle, J. E. 2001, MNRAS, 323, 785

Bonnell, I. A., Vine, S. G., & Bate, M. R. 2004, MNRAS, 349, 735

Elmegreen, B. G. & Lada, C. J. 1977, ApJ, 214, 725

Federrath, C., Banerjee, R., Clark, P. C., & Klessen, R. S. 2010, ApJ, 713, 269

Fryxell, B., Olson, K., Ricker, P., Timmes, F. X., Zingale, M., Lamb, D. Q., MacNeice, P., Rosner, R., Truran, J. W., & Tufo, H. 2000, ApJS, 131, 273

Ho, P. T. P. & Haschick, A. D. 1981, ApJ, 248, 622

Klessen, R. S. & Burkert, A. 2000, ApJS, 128, 287

Kratter, K. M. & Matzner, C. D. 2006, MNRAS, 373, 1563

Krumholz, M. R. & Bonnell, I. A. 2009, in Structure Formation in Astrophysics, ed. G. Chabrier (Cambridge: Cambridge Univ. Press), 288

Krumholz, M. R., Klein, R. I., McKee, C. F., Offner, S. S. R., & Cunningham, A. J. 2009, Science, 323, 754

Motte, F., Bontemps, S., Schneider, N., Schilke, P., & Menten, K. M. 2008, in Astronomical Society of the Pacific Conference Series, Vol. 387, Massive Star Formation: Observations Confront Theory, ed. H. Beuther, H. Linz, & T. Henning, 22–29

Myers, P. C., Dame, T. M., Thaddeus, P., Cohen, R. S., Silverberg, R. F., Dwek, E., & Hauser, M. G. 1986, ApJ, 301, 398

Peters, T., Banerjee, R., Klessen, R. S., & Mac Low, M.-M. 2011, ApJ, 729, 72

Peters, T., Banerjee, R., Klessen, R. S., Mac Low, M.-M., Galván-Madrid, R., & Keto, E. R. 2010a, ApJ, 711, 1017

Peters, T., Klessen, R. S., Mac Low, M.-M., & Banerjee, R. 2010b, ApJ, 725, 134

Peters, T., Mac Low, M.-M., Banerjee, R., Klessen, R. S., & Dullemond, C. P. 2010c, ApJ, 719, 831

Rijkhorst, E.-J., Plewa, T., Dubey, A., & Mellema, G. 2006, A&A, 452, 907

Weidner, C. & Kroupa, P. 2006, MNRAS, 365, 1333

Weidner, C., Kroupa, P., & Bonnell, I. A. D. 2010, MNRAS, 401, 275

Zinnecker, H. & Yorke, H. W. 2007, ARAA, 45, 481